Tuning the nitrogen-doping configuration in carbon materials via sulfur doping for ultrastable potassium ion storage

Yang Xu,[aΔ] Changlai Wang,[b,cΔ] Ping Niu,[a] Zhiqiang Li,[a] Lingzhi Wei,[a] Ge Yao,[a] Fangcai Zheng*[a] and Qianwang Chen**[a,b]

[a] Institutes of Physical Science and Information Technology, Key Laboratory of Structure and Functional Regulation of Hybrid Materials, Anhui University, Ministry of Education, Hefei, 230601, People's Republic of China

[b] Hefei National Laboratory for Physical Science at Microscale and Department of Materials Science & Engineering, University of Science and Technology of China, Hefei 230026, People's Republic of China

[c] Center of Super-Diamond and Advanced Films (COSDAF), Department of Materials Science and Engineering, City University of Hong Kong, Tat Chee Avenue, Kowloon, Hong Kong, People's Republic of China

Corresponding authors: zfcai@mail.ustc.edu.cn (F.C. Zheng)

cqw@ustc.edu.cn (Q. W. Chen)

Y. Xu and Dr. C. Wang contribute equally to this work.

Experiment

Material Synthesis: Nickel chloride ($NiCl_2·6H_2O$,≥98%), nitrilotriacetic acid (NTA, ≥98.5%), isopropanol (≥99.7%), commerical active carbon (AC) and ultrawater were used. All reagents are analytically pure without any further purification.

The Ni-NTA was synthesized by a simple solvothermal method. Firstly, 1.2 g of $NiCl_2·2H_2O$, 0.9 g of nitrilotriacetic acid and 30 mL of isopropanol were mixed in 50 mL Teflon-lined stainless steel autoclave, and then 10 mL of water was added the above solution after stirred 20 min. The stainless steel autoclave was heated at 180 ° C for 6 h. The product was collected by centrifugation, washed with ethanol for three times, and dried at 60 ℃ overnight. The as-prepared Ni-NTA was placed in ceramic boat and annealed at different temperatures (500, 600 and 700 ℃) in N_2 atmosphere with a heating rate of 5 ℃ min^{-1} and kept for 2 h, respectively. Subsequently, the obtained black products were stirred in mixed acids (40 mL of HCl (6 mol L^{-1}) and 40 mL of HNO_3 (3 mol L^{-1})) at 80 ℃ to remove Ni. The corresponding samples were denoted as N-CMs-500, N-CMs-600, and N-CMs-700, respectively. For S/N-CMs, 500 mg of sulfur powder was placed upstream of N-CMs-600 (100 mg) along the N_2 flow direction, which was annealed at 600 ℃ for 2 hours with a heating rate of 5 ℃ min^{-1}.

Material Characterization: The of S/N-CMs were tested with a X-ray power diffraction (XRD) (Rigaku Co, Japan, D/MAX-γA). The surface of samples was observed by scanning electron microscopy (SEM, JEOL JSM-6700 M). Transmission electron microscopy (TEM, Hitachi H-800) and high resolution transmission electron microscopy (HRTEM, JEOL-2011) was used to study the material structure and element distribution of S/N-CMs. The electronic states of related elements were

characterized by X-ray photoelectron spectroscopy (XPS). The degree of defect of porous carbon was characterized by Raman spectra (Via-Reflex/inVia-Reflex). A Shimadzu-50 thermoanalyser (TGA) was used to investigate the thermal behavior of the precursor under flowing N_2 with a heating rate of 20 ^oC min^{-1}.

Electrochemical Measurements: The cell was assembled with CR2032 coin cells at a glovebox filled with Argon atmosphere ($O_2 \leq 0.01$ ppm, $H_2O \leq 0.01$ ppm). To prepare the electrode, the active material was mixed with acetylene black and Polyvinylidene Fluoride (PVDF) at ratio 8:1:1 in N-methyl pyrrolidone (NMP) to form uniform slurry. The slurry was loaded on the Cu foil and then dried at 80 °C for 24 h in a vacuum drying oven. The metal potassium is employed as cathode electrode, and the electrolyte was a solution of 3 mol L^{-1} KFSI in EC:DC = 1:1. The electrode loading mass is around 0.4 mg. For potassium ion capacitor, S/N-CMs-600 coated on Al foil was served as the anode and commercial activated carbon (Alladdin) was served as the cathode. The mass ratio for anode and cathode is 1:2. Cyclic voltammetry (CV) and electrochemical impedance spectroscopy (EIS) were performed on CHI760E electrochemical workstation. The galvanostatic charge/discharge measurements and Galvanostatic Intermittent Titration Technique were conducted on Neware CT3008W.

Theoretical calculations: All theoretical calculations were performed based on density functional theory (DFT), as implemented in the Vienna ab-initio simulation package (VASP).[1] The exchange-correlation interactions were treated by The Perdew-Becke-Ernzerhof (PBE) [2] functional. The projector augmented wave (PAW) [3] was used with a kinetic energy cutoff of 400 eV. All structures were optimized with a convergence criterion of 1×10^{-5} eV for the energy and 0.01 eV/Å for the forces. The first Brillouin zone was sampled by a 3×3×3 k-point grid generated within the Monkhorst-Pack [4] scheme.

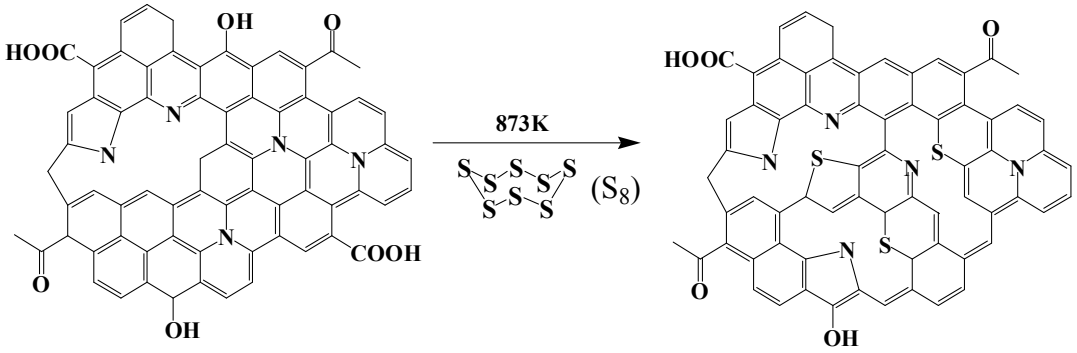

Scheme S1. The scheme for the formation of S/N-CMs-600.

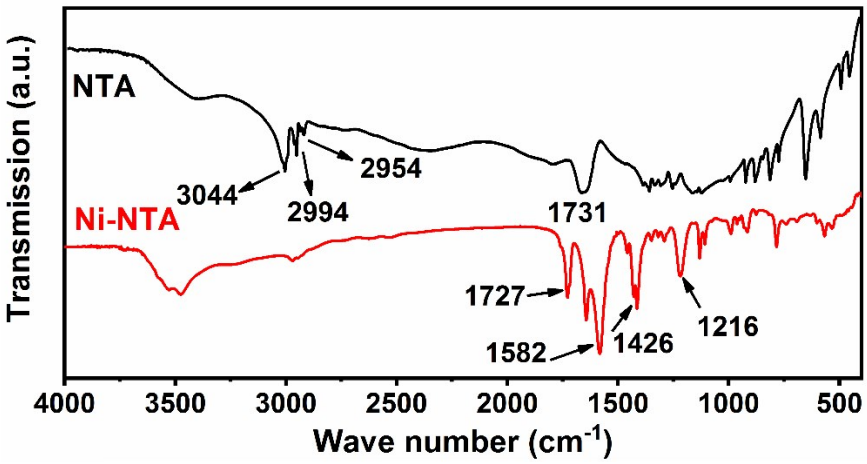

Figure S1. FTIR spectra of Ni-NTA and NTA.

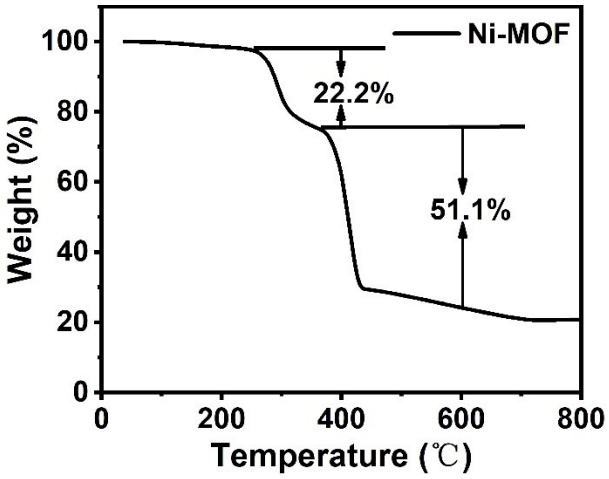

Figure S2. TG curves of Ni-NTA.

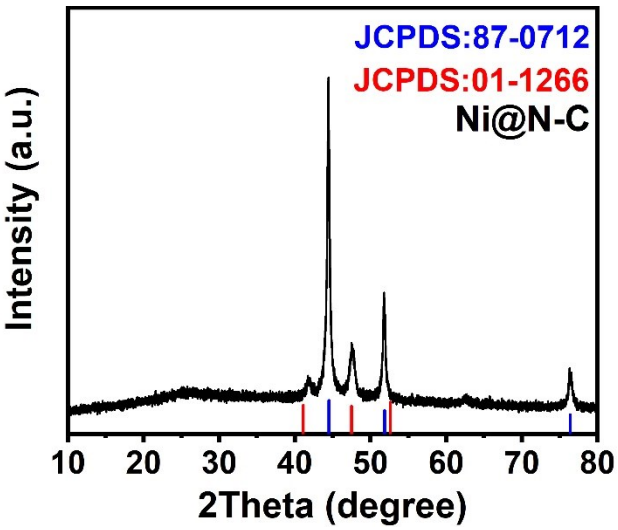

Figure S3. XRD pattern of Ni@N-C.

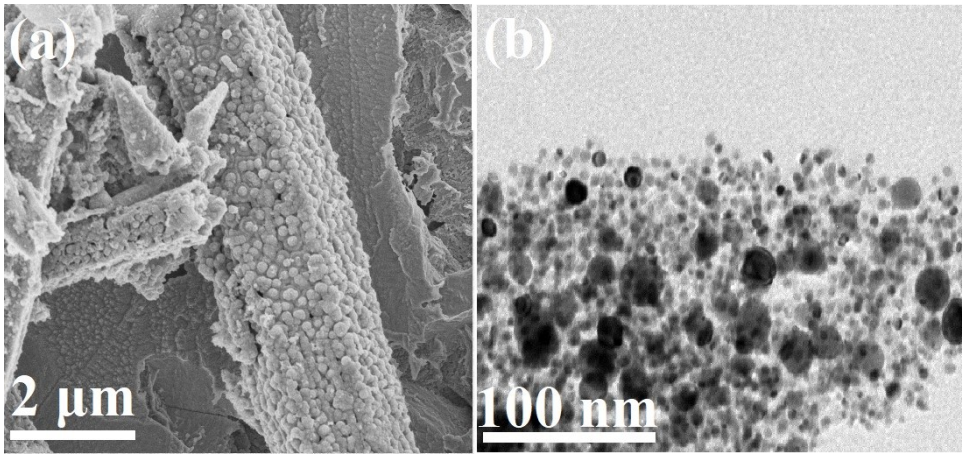

Figure S4. SEM and TEM images of Ni@N-C.

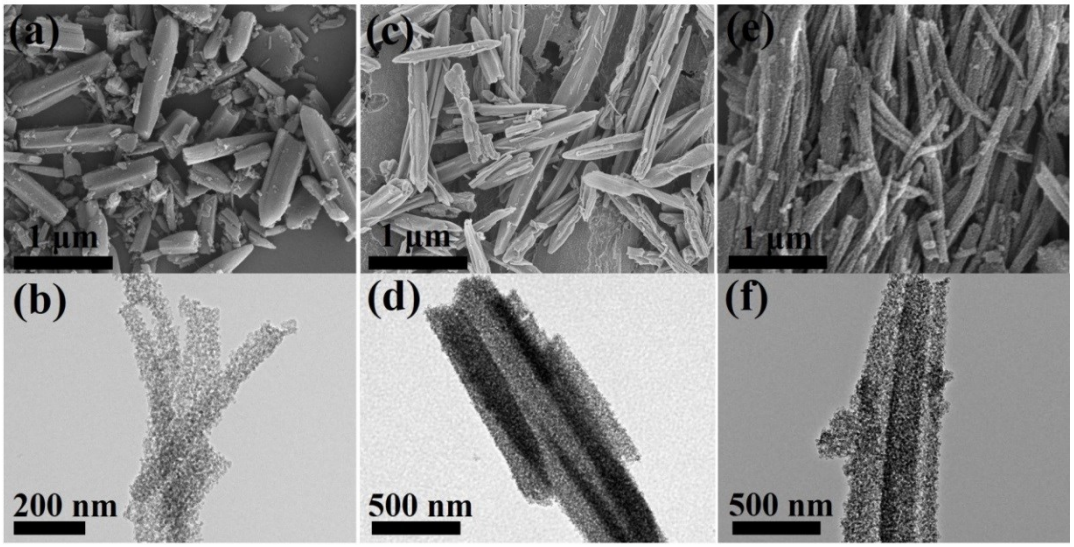

Figure S5. SEM and TEM images of (a,b) N-CMs-500, (c,d) N-CMs-600 and (e,f) N-CMs-700.

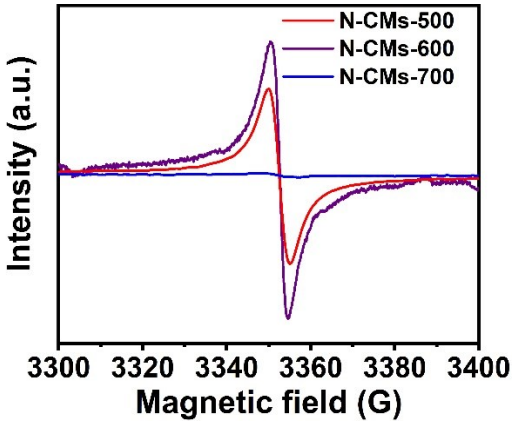

Figure S6. EPR spectra for N-CMs-500, N-CMs-600 and N-CMs-700.

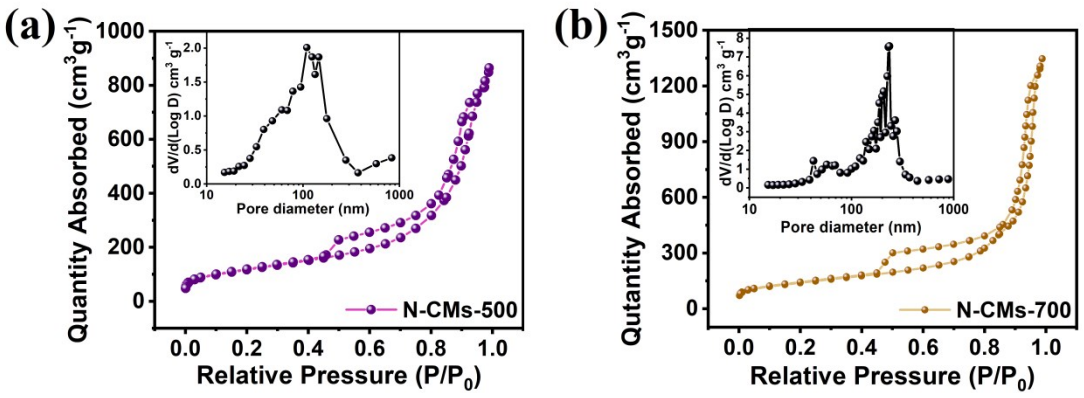

Figure S7. N_2 adsorption-desorption isotherms and pore size distribution of (a) N-CMs-500 and (b) N-CMs-700.

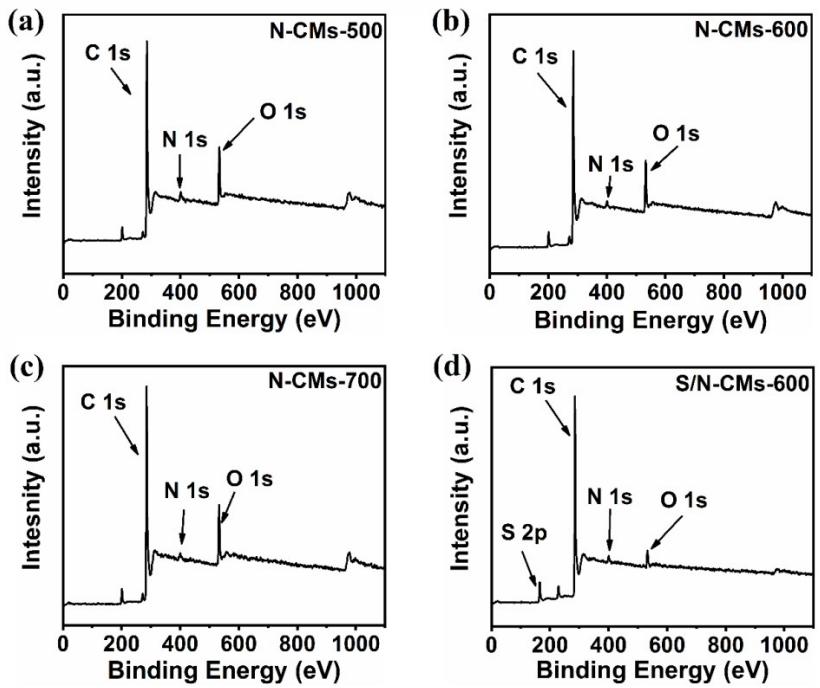

Figure S8. XPS survey of N-CMs-500, N-CMs-600, N-CMs-700 and S/N-CMs-600.

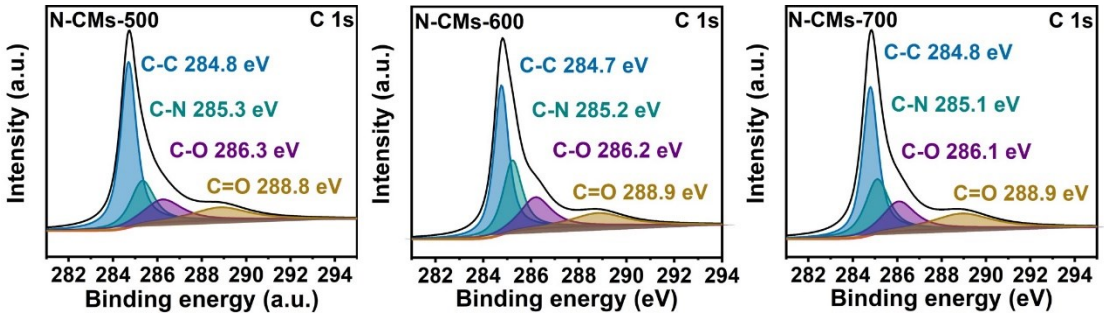

Figure S9. C 1s spectra for (a) N-CMs-500, (b) N-CMs-600 and (c) N-CMs-700.

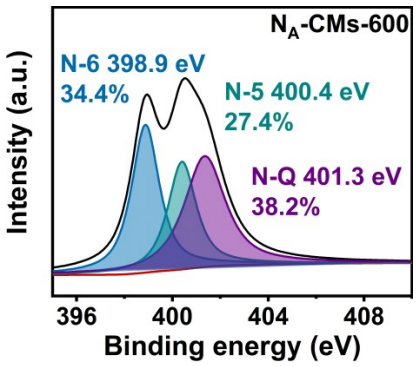

Figure S10. The N1s spectura of N_A-CMs-600

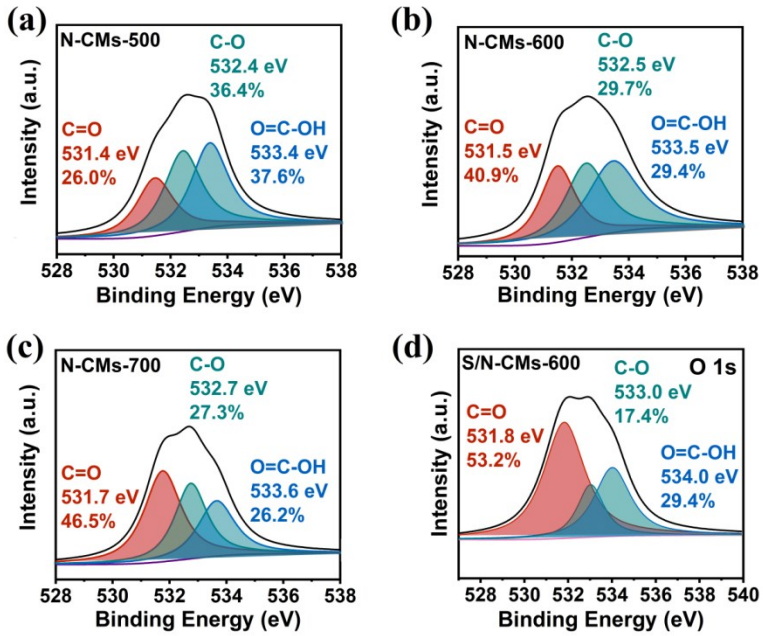

Figure S11. O 1s spectra for (a) N-CMs-500, (b) N-CMs-600, (c) N-CMs-700 and (d) S/N-CMs-600.

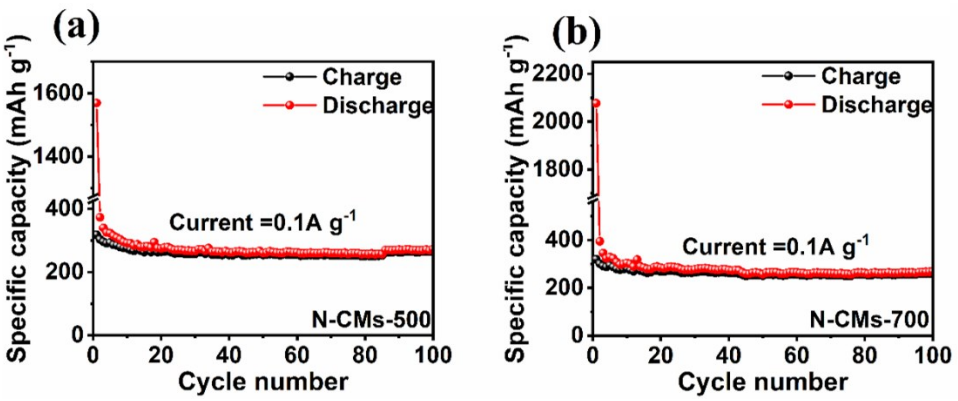

Figure S12. Cycling performances of (a) N-CMs-500 and (b) N-CMs-700 at 0.1 A g^{-1}.

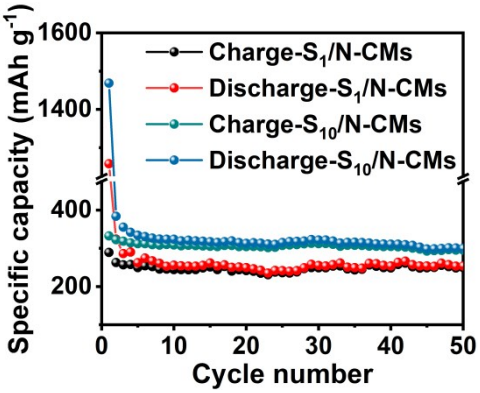

Figure S13. Cycling performances of S_1/N-CMs and S_{10}/N-CMs at 0.1 A g^{-1}.

To further explore the effect of the sulfur content on the potassium storage performance, the different ratios (1:1 and 10:1) of the sulfur powder and N-CMs-600 were shose to synthesize S/N-CMs, and the coresponding samples were donoted as S_1/N-CMs and S_{10}/N-CMs. As shown in Figure S12, the S_{10}/N-CMs (298.5 mAh g^{-1} at 0.1 A g^{-1} over 50 cycles) displays a higher capacity than that S_1/N-CMs (248.6 mAh g^{-1} at 0.1 A g^{-1} over 50 cycles), indicating that the increase of sulfur content contributes to the potassium storage performance. However, the potassium storage capacities of S_1/N-CMs and S_{10}/N-CMs are lower than that of N-CMs-600 (441.5 mAh g^{-1} at 0.1 A g^{-1} over 100 cycles) synthesized with 5:1 of the sulfur powder and N-CMs-600.

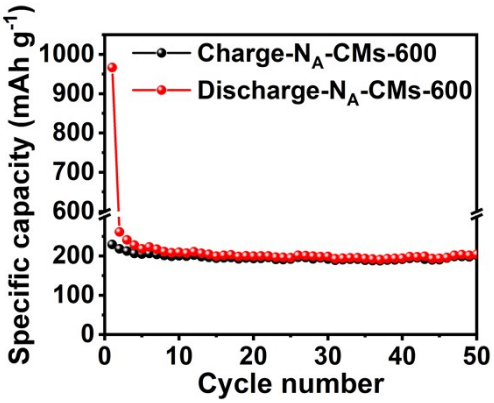

Figure S14. The cycle performances of N_A-CMs-600 at 0.1 A g^{-1}.

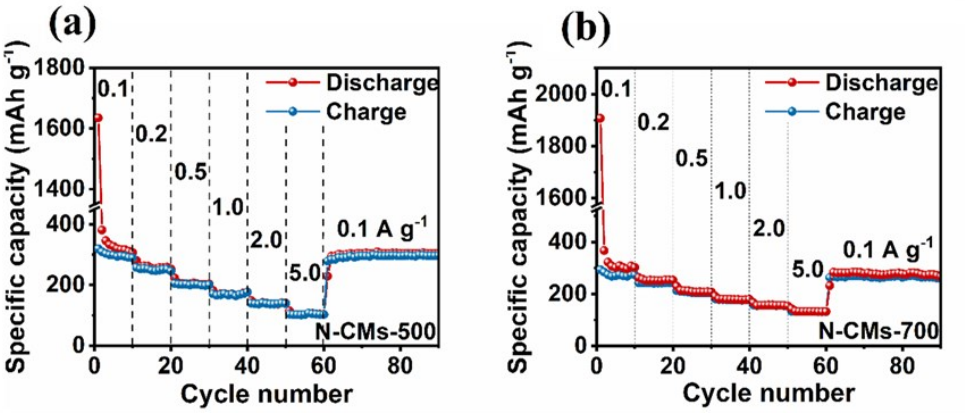

Figure S15. Rate performances of (a) N-CMs-500 and (b) N-CMs-700.

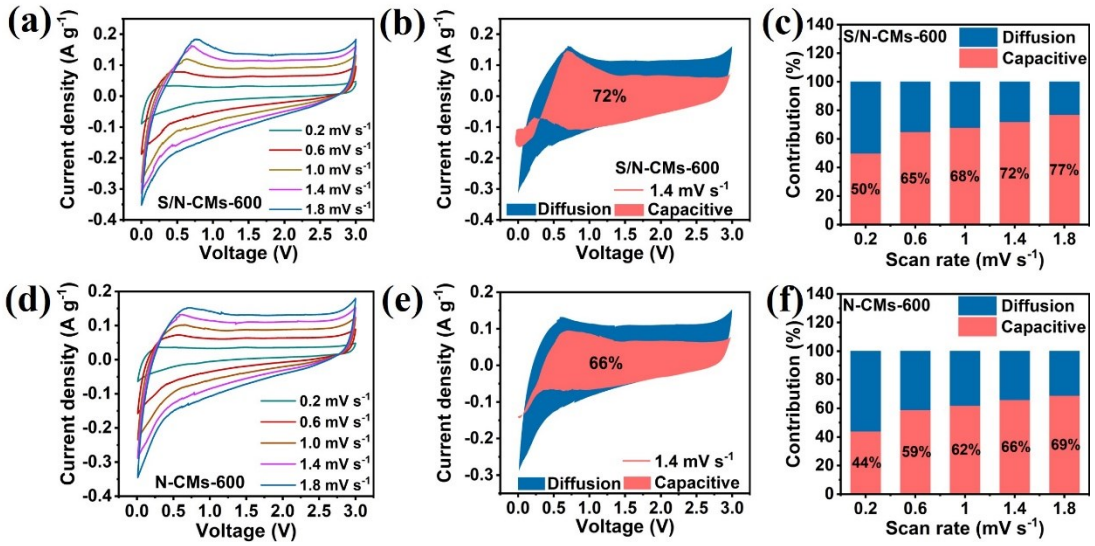

Figure S16. CV curves of (a) S/N-CMs-600 and (d) N-CMs-600 at different scan rates from 0.2 to 1.8 mV s^{-1}. Capacitive contribution ratios of (b) S/N-CMs-600 and (e) N-CMs-600 at 1.4 mVs^{-1}. Capacitive contribution ratios of (c) S/N-CMs-600 and (f) N-CMs-600 at different scan rates.

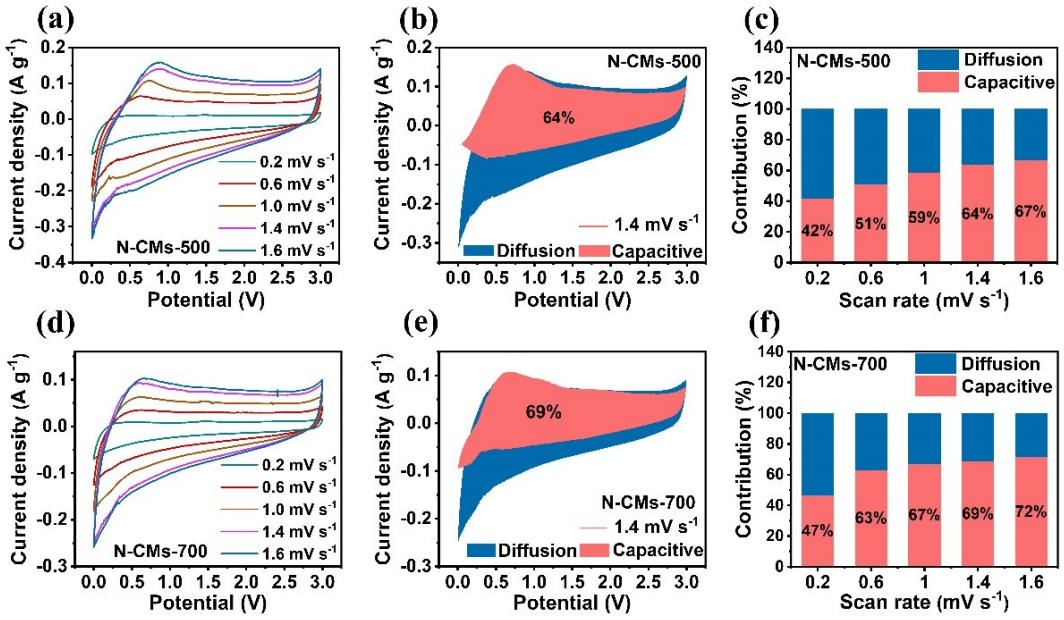

Figure S17. CV curves of (a) N-CMs-500 and (d) N-CMs-700 at different scan rates from 0.2 to 1.8 mV s^{-1}. Capacitive contribution ratios of (b) N-CMs-500 and (e) N-CMs-700 at 1.4 mVs^{-1}. Capacitive contribution ratios of (c) N-CMs-500 and (f) N-CMs-700 at different scan rates.

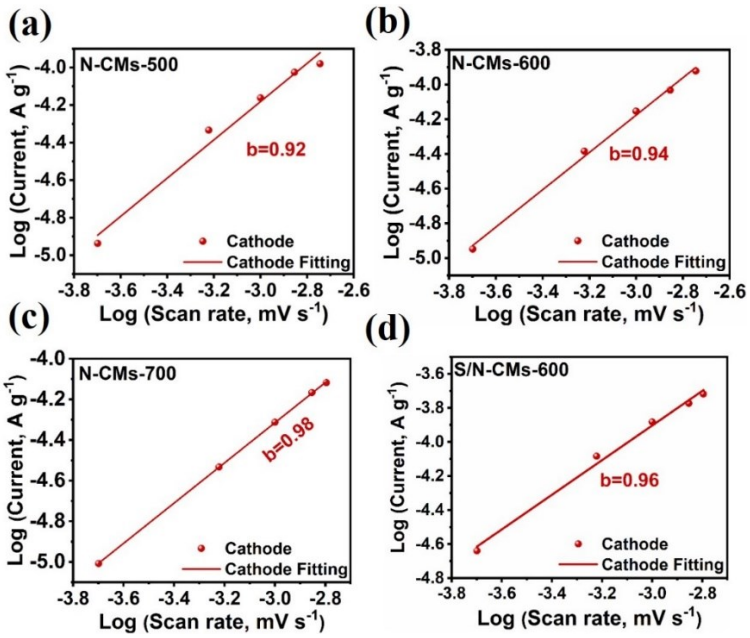

Figure S18. Slope fitting of b values for (a) N-CMs-500, (b) N-CMs-600, (c) N-CMs-700 and (d) S/N-CMs-600.

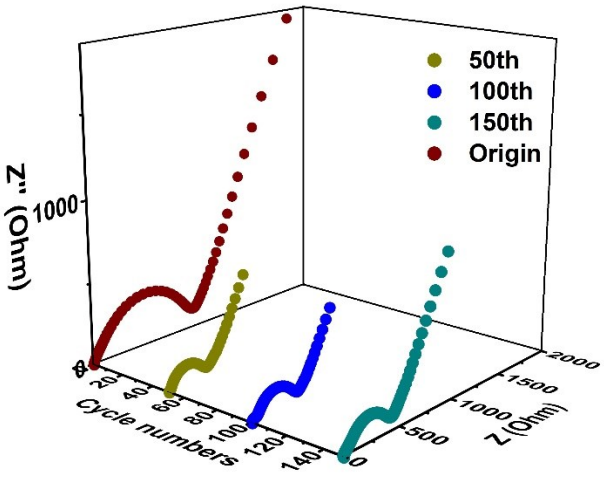

Figure S19. The Nyquist plots of S/N-CMs-600 after different cycles

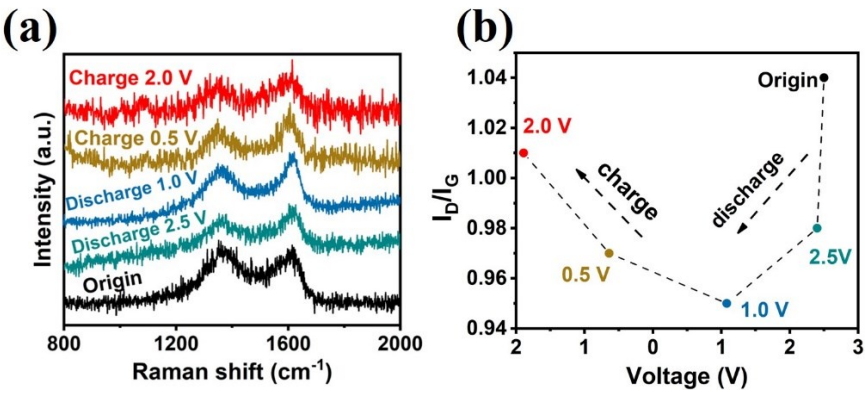

Figure S20. (a) Ex-situ Raman of S/N-CMs-600 at different voltages. (b) the I_D/I_G value changes accord to voltage changes

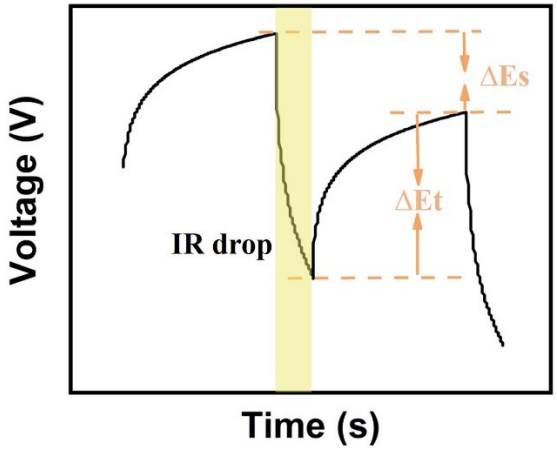

Figure S21. Schematic of the calculation of diffusion coefficient using the GITT technique.

Galvanostatic intermittent titration technique (GITT) is also employed to study the diffusion coefficient of K-ion in S/N-CMs-600 at 0.1 A g^{-1} for 0.2 h between rest intervals for 0.7 h. The diffusion coefficient can be calculated according to Fick's second law as follows [5]:

$$D = \frac{4}{\pi\tau}\left(\frac{m_B V_M}{M_B S}\right)^2\left(\frac{\Delta E_s}{\Delta E_\tau}\right)^2$$

Here, τ is the pulse time, M_B is molar mass of material, m_B and S are the active mass and surface area for the test sample, V_M is the molar volume, ΔE_S and ΔE_τ can be obtained from our test results.

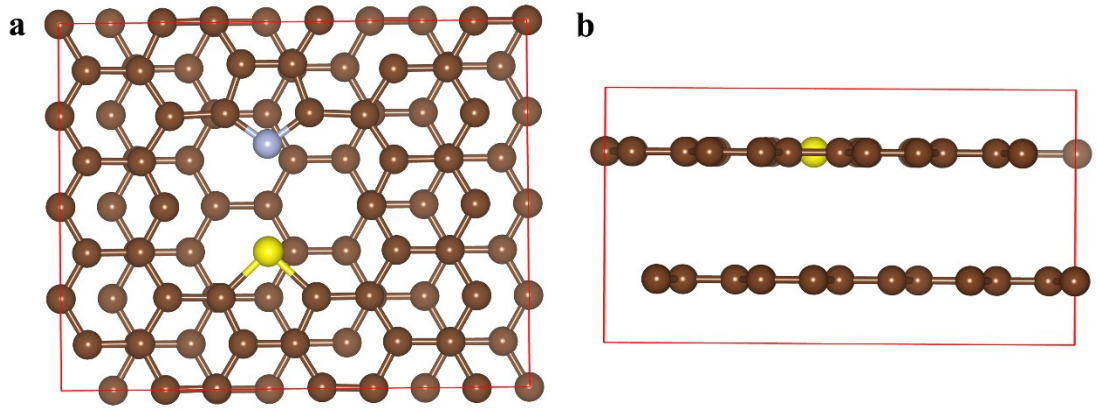

Figure S22. The model of pyrrolic N with S dual-doped carbon (N_5SC). (a) Top view (b) side view. The brown, grey, and yellow balls represent C, N, and S atoms, respectively.

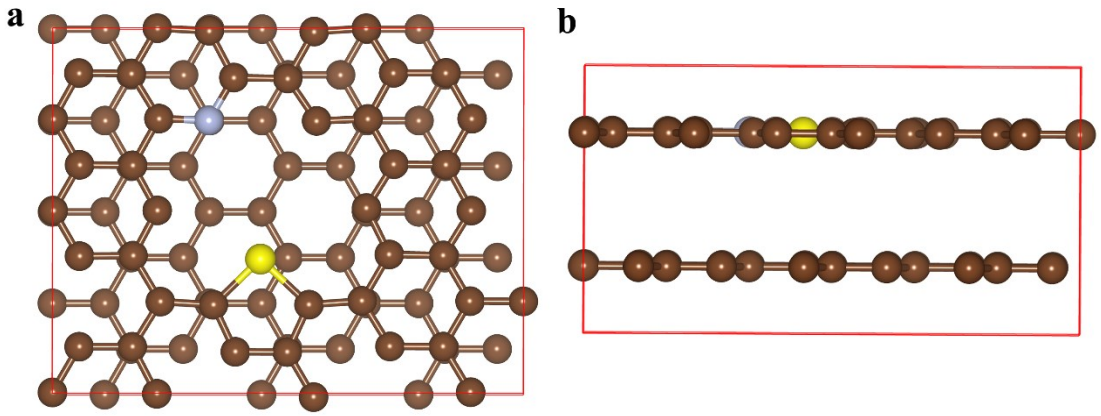

Figure S23. The model of pyridinic N with S dual-doped carbon (N_6SC). (a) Top view (b) side view. The brown, grey, and yellow balls represent C, N, and S atoms, respectively.

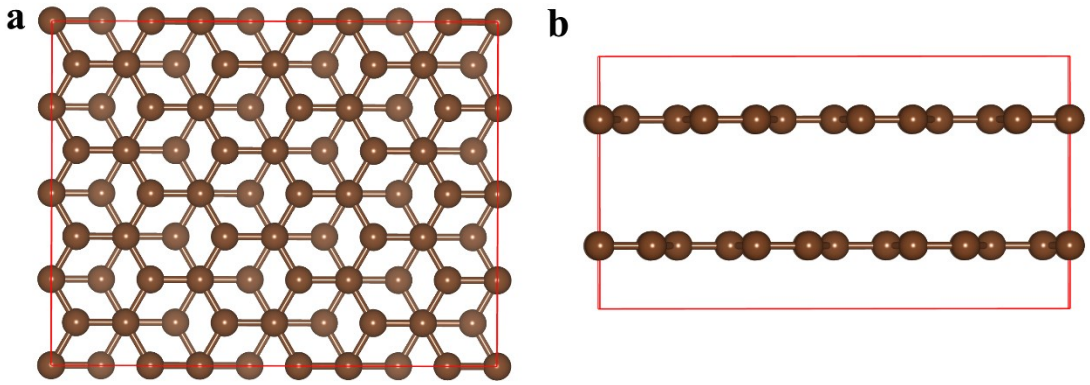

Figure S24. The model of pristine carbon. (a) Top view (b) side view. The brown ball is C atom.

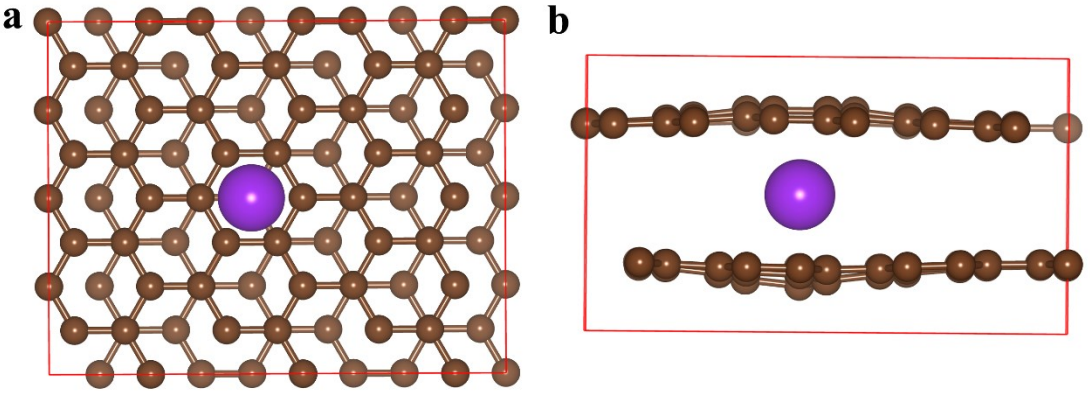

Figure S25. The structure of K intercalating into pristine carbon from top view (a) and side view (b). The brown and purple balls are C and K atoms, respectively.

Table S1. BET surface areas and pore features of samples.

Samples	Specific area ($m^2 g^{-1}$)	Pore volume ($cm^3 g^{-1}$)	Pore diameter (nm)
N-CMs-500	511.24	1.288	7.812
N-CMs-600	621.87	1.661	8.480
N-CMs-700	642.69	2.037	9.839
S/N-CMs-600	473.98	1.165	8.561

Table S2. Comparison of the cycling stability in this work with previously reported carbon materials.

Samples	Current density ($mA g^{-1}$)	Cycle number	Capacity ($mAh g^{-1}$)	Ref.
N/S dual-doped carbon	1000/100	1000/200	178.0/359.0	6
N-doped porous carbon	500/50	1000/100	121.3/296.8	7
Biomorphic-based N-doped carbon	1000/100	1000/200	74.1/263.6	8
N/S co-doped carbon	1000/100	1000/100	249.5/321.3	9
Hollow carbon bowls	1000/100	1000/150	133.0/304.1	10
Sulfur and nitrogen codoped carbon nanofiber	2000/500	1000/200	168.0/191.0	11
N/S co-doped graphene	1000/100	2000/200	188.8/251.2	12
S/N-CMs-600	2000/100	1000/100	283.3/441.5	This work

References

[1] G. Kresse and J. Hafner, *Phys Rev B.,* 1993, **48**, 13115.

[2] J. P. Perdew, K. Burke and M. Ernzerhof, *Phys Rev Lett.,* 1996, **77**, 3865.

[3] G. Kresse and D. Joubert, *Phys Rev B.,* 1999, **59**, 1758.

[4] H. J. Monkhorst and J. D. Pack, *Phys Rev B.,* 1976, **13**, 5188.

[5] L. Tao, Y. P. Yang, H. L. Wang, Y. L. Zheng, H. C. Hao, W. P. Song, J. Shi, M. H. Huang and D. Mitlin, *Energy Storage Mater.,* 2020, **27**, 212-225.

[6] Q. D. Liu, F. Han, J. F. Zhou, Y. Li, L. Chen, F. Q. Zhang, D. W. Zhou, C. Ye, J. X. Yang, X. Wu and J. S. Liu, *ACS Appl. Mater. Interfaces,* 2020, **12**, 20838-20848.

[7] X. J. Qi, K. S. Huang, X. Wu, W. Zhao, H. Wang, Q. C. Zhuang and Z. C. Ju, *Carbon,* 2018, **131**, 79-85.

[8] C. L. Gao, W. G. Qing, S. H. Luo, Z. Y. Wang, Y. H. Zhang, Y. G. Liu, A. M. Hao, R. Guo, *J. Power. Sources,* 2019, **415**, 165-171.

[9] B. B. Fan, J. X. Yan, A. P. Hu, Z. Liu, W. Z. Li, Y. H. Li, Y. L. Xu, Y. Zhang, Q. L. Tang, X. H. Chen and J. L. Liu, *Carbon,* 2020, **164**, 1-11.

[10] Z. L. Zhang, B. R. Jia, L. Liu, Y. Z. Zhao, H. Y. Wu, M. L. Qin, K. Han, W. A. Wang, K. Xi, L. Zhang, G. G. Qi, X. H. Qu and R. V. Kumar, *ACS Nano,* 2019, **13**, 11363-11371.

[11] C. X. Lv, W. J. Xu, H. L. Liu, L. X. Zhang, S. Chen, X. F. Yang, X. J. Xu, D. J. Yang, Small, 2019, **15**, 1900816.

[12] W. X. Yang, J. H. Zhou, S. Wang, Z. C. Wang, F. Lv, W. S. Zhang, W. Y. Zhang, Q. Sun and S. J. Guo, *ACS Energy Lett.,* 2020, **5**, 1653-1661.